Laser-Assisted Bonding for Micro-LED Modules in Head-Up Display Applications

Wenya Tian*, Yiran Wu*, Yuanhao Sun*, Peilin Zhang*, Yatong Qiao*, Ming Chen*

***BOE TECHNOLOGY GROUP CO., LTD, Beijing, China**

Abstract

The mass transfer process is a critical aspect of microLED technology, with the metal interconnect between the chip and substrate as a key bottleneck. Laser-assisted eutectic bonding improved photoelectric efficiency by 51.3%, enabling the realization of a 3.8-inch, 1280×1024 ultra-high-resolution HUD display module with a lighting yield exceeding 99.9%, accelerating Micro-LED commercialization.

Author Keywords

Micro-LED display; Laser-assisted bonding; HUD; Micro-morphology.

1. Introduction

Micro-LED technology, with its high reliability, long lifespan, fast response time, and high brightness, has emerged as a leading candidate for next-generation display technology [1,2]. After over 20 years of development, Micro-LED has made significant progress, with mass-produced products now available in ultra-large commercial displays, ultra-small AR/VR displays, and medium-sized transparent displays, including head-up displays (HUDs) for automotive applications. HUDs are expected to become a primary interface for human-machine interaction in future vehicles, with augmented reality (AR) enhancing the HUD experience and accelerating the shift away from traditional instrument clusters. As adoption rates rise and supply chains mature, the cost of HUDs is expected to decrease, potentially reaching the USD 150–200 range. By 2025, the Chinese HUD shipment market is projected to grow 3.5 times, reaching approximately USD 1.4 billion compared to 2022 [3,4].

One of the key challenges in the large-scale production of Micro-LED displays is the efficient and reliable bonding of Micro-LEDs to substrates. Laser-assisted bonding (LAB) has emerged as a promising solution for Micro-LED transfer, offering significant advantages in welding speed, precision, and thermal management. By precisely controlling infrared lasers, LAB enables rapidly heating and cooling of the solders, achieving faster welding speeds and minimizing heat damage. LAB also enables micron-scale, single-point welding, which is critical for meeting the high-precision requirements of Micro-LED assembly. The short heating time reduces the heat-affected zone, minimizing thermal and vibrational stresses, and significantly improving welding quality and reliability[5,6,7].

In contrast, traditional bonding methods such as anisotropic conductive film (ACF) bonding and thermocompression bonding have certain limitations. ACF bonding, which operates at room temperature, avoids thermal mismatch but suffers from low transfer efficiency and challenges in repair. Thermocompression bonding, while compatible with laser technology in efficiency, is hindered by thermal mismatch and longer processing times. LAB, with its high efficiency, precision, and reduced thermal damage, is thus seen as the most promising solution for large-scale Micro-LED transfer.

This research investigates a solid-liquid low-temperature LAB bonding method using a 980 nm laser for 1280×1024 Micro-LED arrays with Sn bumps. The principles of solid-liquid bonding are explored in detail, and optimization of laser energy and process parameters is performed to achieve a metal bonding interface with nearly 100% filling rate. This approach demonstrates lower contact resistance and superior shear strength compared to thermocompression bonding. Additionally, the electrical and optical parameters of the Micro-LED array are tested.

2. Experimental procedures

In this study, an 18×40 μm Micro-LED chip with a patterned sapphire substrate (PSS) structure and a thickness of 7 μm was used. The devices, spaced at a pitch of 58.88 μm, were placed on a sapphire substrate (COW). Initially, a temporary thermo-compression bonding technique was applied to attach the COW chip to a substrate without alignment. Next, a KrF excimer laser (248 nm) was used to remove the sapphire substrate (Fig. 1(b-c)), a process referred to as chip on carrier-1 (COC-1). The chips on COC-1 were then transferred to COC-2, maintaining the same pitch, with the devices positioned with the electrodes facing outward (Fig. 1(d)).

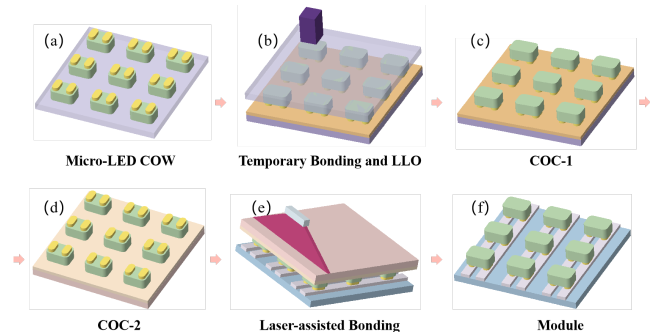

Figure 1. Schematic of the process Flow.

Afterward, COC-2 was aligned with a flux-coated driving backplane, adjusted to a perfectly parallel state, and slowly pressed into contact with pressure sensors monitoring the force between them (Fig. 1(e)). A strip-shaped infrared laser passed through the COC-2 interlayer to heat and melt the solder, with the laser spot moving at a fixed speed, allowing the molten solder to form a eutectic alloy with the Ni metal. The strength between the chip and backplane, created by the eutectic alloy, exceeded the adhesion between the chip and COC-2, enabling easy removal of the COC-2 substrate and completing the laser-assisted bonding (LAB) process (Fig. 1(f)). This process resulted in a high-brightness display module with a resolution of 1024×1280, producing a 3.8-inch monochrome green display with a 58.88 μm pixel pitch. The laser illuminated both the p- and n-electrodes of the Micro-LED chip simultaneously, eliminating electrode stress adaptation issues by preventing a significant temperature gradient. Additionally, the LAB process involved a considerably short heating time, effectively minimizing thermal expansion and substrate warping due to thermal mismatch between the substrates, which significantly enhanced yield and display performance.

ISSN 0097-996X/25/5602-0818-$1.00 © 2025

3. Results and Discussion

3.1 Optimization of Micro-LED Laser Bonding Process

Due to the circular deep-hole design of the N-type layer of the Micro-LED chip, the surface of the N-electrode metal exhibits a pit-like structure, resulting in macroscopic voids between the electrode and the backplane pad. These voids can lead to issues such as virtual connections and low reliability after laser bonding. To address these problems, this study adjusts the pressure and laser energy during the welding process, ultimately achieving a well-welded interface with a metal filling rate of 99.99% (Fig. 2(a–e)). The metal filling rate is calculated by subtracting the void rate from 100%. Adjusting the pressure leads to changes in the gap between the COC-2 and the backplane, while altering the laser energy affects the temperature variation at the welding interface. These adjustments are reflected in the gap and temperature values plotted in the graphs. Figure 2(f) summarizes the relationship between the metal filling rate at the welding interface, the gap, and the temperature. Optimal soldering, with no voids, is achieved when the gap is 15 μm and the temperature is 260°C.

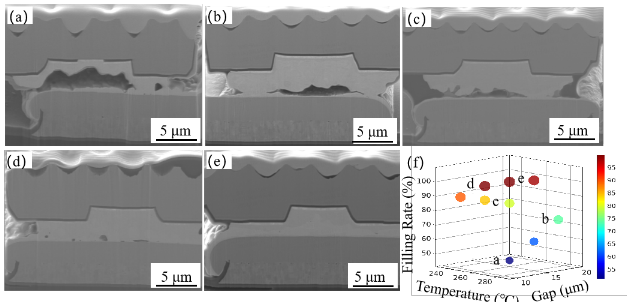

Figure 2. Interface morphology of solder joints under different pressures and temperatures.

With the optimized condition, the solder metallization establishes the electrical connection between the Micro-LED and the backplane, completing the chip packaging process for a 1280×1024 monochrome green display module. The laser bonding success rate for the entire display module exceeds 99.9%, and the chips and backplane are not damaged by the laser radiation. The appearance of the welded chips in local areas and the cross-sectional view of the entire chip are shown in Fig. 3.

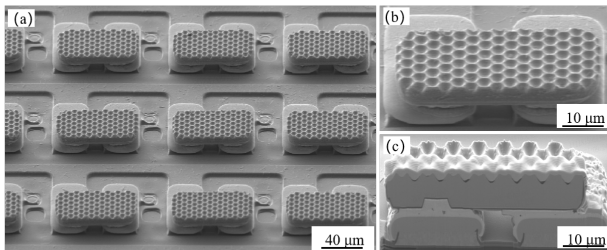

Figure 3. Appearance of the Micro-LED chip after metal interconnection with the backplane.

3.2 Mechanism of Solid-liquid Inter-diffusion and Eutectic Alloy Formation

The physical process of Sn/Au/Ni bonding is illustrated in Fig. 4. When sufficient pressure is applied to bring the chip pad and substrate into close contact at a temperature above the melting point of Sn (232°C), solid-liquid diffusion occurs, as shown in Fig. 4(b). In its molten state, Sn wets the adjacent Au and Ni layers, forming an alloy as the liquid and solid components inter-diffuse. This mixture remains in direct contact with the Au and Ni layers on the surfaces to be joined, wetting and dissolving these layers until the mixture solidifies to form a Ni-Au-Sn bond (Fig. 4(c)).

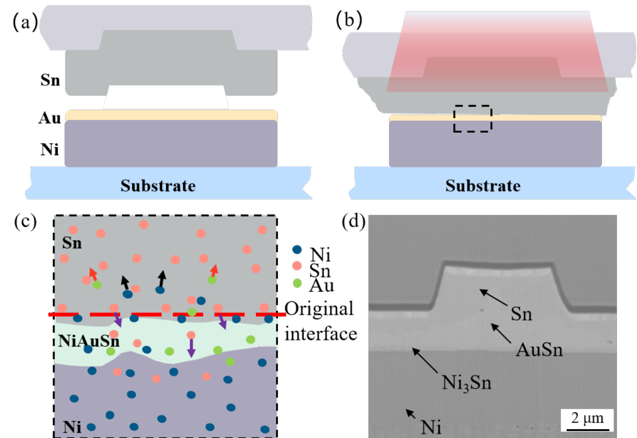

Figure 4. Bonding process description. (a) Alignment of the metal solder joints (b) Laser-assisted bonding (c) Melting of Sn and solid-liquid inter-diffusion (d) Solidification and solid-state diffusion.

As the process progresses, the interaction between Sn and Au becomes faster and more noticeable. In the Au/Sn structure, The Sn layer melts and fully dissolves the thin Au layer, reacting with the thicker Au layer beneath it to form the (L) phase, as predicted by the gold-tin equilibrium phase diagram. The (L) phase eventually moves below the liquidus line and transitions into a molten phase with AuSn compound grains, forming an intermetallic compound AuSn with a 1:1 atomic ratio and reaching a stable state. This intermetallic compound is characterized by low resistance. The molten metal rapidly fills the macroscopic pit structure, causing the interfacial voids to gradually disappear and improving the electrical connection reliability of the eutectic interface. Sn atoms migrate to the Ni interface, which has a lower chemical diffusion potential energy and greater stability, forming a relatively stable Ni3Sn compound. The diffusion of Ni atoms is suppressed due to their relative stability, and the Ni3Sn compound forms primarily near the interface. The entire metal bonding interface consists of four layers, from top to bottom: a pure Sn layer, an AuSn compound layer, a Ni3Sn eutectic metal layer, and a Ni atomic metal layer (Fig. 4(d)).

3.3 Enhanced Optoelectronic Performance of Metal Eutectic Bonded Devices

By comparing display modules with metal eutectic bonding to those bonded with ACF, it is clear that the laser-bonded modules achieve a current efficiency of 60 cd/A, which is approximately 1.5 times higher than that of the ACF-bonded samples. This improvement is attributed to the absence of photon absorption by the ACF film. As shown in Fig. 5(a), the current for a single chip at a brightness of 100,000 nits increases from 5.2 μA in eutectic samples to 7.9 μA in ACF samples, resulting in a 34.2% reduction in power consumption for devices bonded using laser bonding. Additionally, at a Vdd-to-Vss voltage difference of 11.5 V, the voltage across the LED chip post-eutectic bonding stabilizes around 3.5 V with a current of 9.5 μA, indicating the normal operating output for the display module, as confirmed by the LED IV curve and TFT Vds-I curve (Fig. 5(c)).

The sparse conductive particles in ACF bonding result in higher contact resistance between the metal connections, causing a larger voltage drop (4.6 V) across the LED terminals under the same drive

current. This increases the slope of the I-V curve, shifting the TFT from the saturation region to the linear region, which in turn reduces the TFT's output current. The high resistance and voltage drop in ACF bonding require a higher Vdd-to-Vss voltage to maintain saturation in the drive circuit, leading to increased power consumption.

Metal eutectic bonding mitigates the negative effects of ACF's high resistance, such as reduced energy efficiency, degraded display quality, and poor wavelength shift uniformity. Also, the luminous viewing angle demonstrates better symmetry on both sides with metal eutectic bonding (Fig. 5(d)), although further optimization of optical encapsulation is needed to address the remaining brightness variation at the frontal viewing angle.

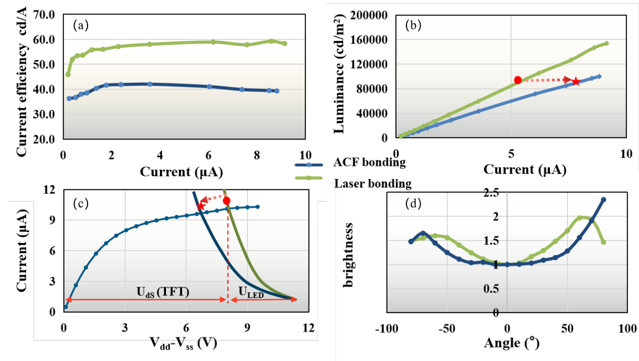

Figure 5. (a) Efficiency–current curve and (b) Luminance–current curve of the devices. (c) I-V curve of the TFT and LED. (d) Brightness distribution with respect to the viewing angle.

3.4 Display Module and Optical System

A 3.8-inch, 1280×1024 pixel green display, integrated with a Micro-LED array on TFT glass, is designed for automotive HUD applications. It operates at a 60 Hz refresh rate and achieves a peak brightness exceeding 100,000 nits, ensuring optimal visibility in bright environments. This high brightness, combined with a dominant wavelength of 525 nm and a contrast ratio of 400:1, meets the demanding requirements of smart driving systems.The active area of the display uses a 7T1C circuit to control and drive the analog signal. When a scan signal is applied to the addressing transistor gate, it activates, allowing the data signal to pass through to the driving transistor gate while storing data in the capacitor. By coordinating external driving signals and timing sequences, the display reliably presents key information such as navigation and speed.

Figure 6. Different display effect of the 3.8-inch module.

As shown in Figure 7, this display has been successfully integrated into an HUD optical system, offering high resolution and brightness for stable operation in various lighting conditions. The improved brightness addresses a common challenge faced by previous HUD systems, which struggled to achieve sufficient brightness for practical use, especially in bright outdoor environments. With the help of the Micro-LED module, the HUD system enables real-time display of essential information, such as navigation and speed, minimizing the need for the driver to divert attention from the road. By presenting key data within the driver's line of sight, HUDs enhance situational awareness and support more accurate assessments of road conditions, potentially improving driving safety.

Figure 7. HUD optical system.

4. Summary

Laser-assisted bonding technology has been utilized to enable the integration of Micro-LED chips with the backplane. A detailed analysis of the eutectic alloy formation process, examining its relationship with temperature and pressure parameters, was conducted to optimize eutectic performance and significantly enhance the reliability of metal solder joints. Comparative testing and characterization reveal the distinct photoelectric advantages of metal eutectic display modules over those bonded with ACF. A 3.8-inch, 1280×1024 ultra-high-resolution, ultra-high-brightness HUD display module was successfully developed, achieving a lighting yield exceeding 99.9%. Leveraging this high-brightness display module, a transmissive HUD optical-mechanical system has also been developed, marking a significant advancement in the field.

5. References

1. Yang Q , Yang Z , Lan Y F ,et al.Low-diffraction transparent micro light-emitting diode displays with optimized pixel structure[J].Journal of the Society for Information Display, 2022(4/6):30.
2. Liu M , Nie J , Liu Y ,et al.Research on the reliability of Micro LED high-density solder joints under thermal cycling conditions[J].IOP Publishing Ltd, 2022.
3. Horng R H , Chen Y F , Wang C H ,et al.Development of Metal Bonding for Passive Matrix Micro-LED Display Applications[J].IEEE Electron Device Letters, 2021(7):42.
4. Joo H S , Lee C J , Min K D ,et al.Mechanical properties and microstructural evolution of solder alloys fabricated using laser-assisted bonding[J].Journal of Materials Science: Materials in Electronics, 2020, 31(24):1-7.
5. Hun C J , Lee S J , Kwon K O ,et al.A monolithically integrated micro-LED display based on GaN-on-silicon substrate[J].Applied Physics Express, 2020, 13(2):026501
6. Tian W Y, Ma Z, Cao X, et al. Application of metal interconnection process with micro-LED display by laser-assisted bonding technology[J]. Journal of Materials Science: Materials in Electronics, 34(35): 2253.
7. Temel O , Kalay Y E , Akin T .Wafer-Level Low-Temperature Solid-Liquid Inter-Diffusion Bonding With Thin Au-Sn Layers for MEMS Encapsulation[J].Journal of Microelectromechanical Systems: A Joint IEEE and ASME Publication on Microstructures, Microactuators, Microsensors, and Microsystems, 2021(30-1).